PREPRINT UCRL-79731

CONF-771136--22

Lawrence Livermore Laboratory

EXPLODING PUSHER TARGETS FOR THE SHIVA LASER SYSTEM

M. D. Rosen, J. T. Larsen, and J. H. Nuckolls

September 26, 1977

This paper was prepared for presentation at the 19th Annual Meeting of the American Physical Society/Division of Plasma Physics, Atlanta, Georgia, November 6-11, 1977.

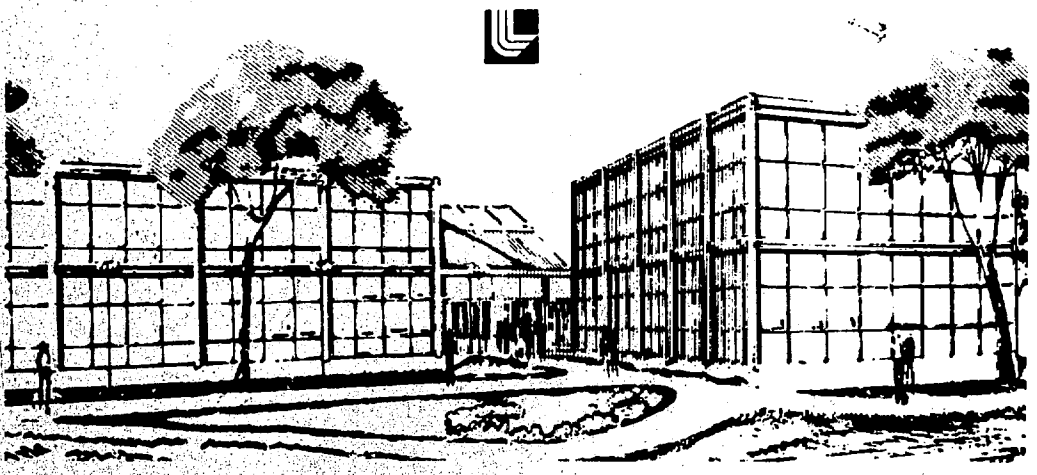

EXPLODING PUSHER TARGETS FOR THE SHIVA LASER SYSTEM*

M. D. Rosen, J. T. Larsen, and J. H. Nuckolls

University of California, Lawrence Livermore Laboratory
Livermore, California 94550

ABSTRACT

We have designed the first targets for the 20 TW SHIVA laser system. They are simple glass micro-balloons, approximately 300 μm in diameter and 2 μm thick, filled with D-T gas. Using LASNEX, whose model physics was utilized successfully for ARGUS targets, we optimize for both gain and yield. The target behaves as an exploding pusher. Different simple analytic models for the physics of this mode are presented, and are tested by comparing their scaling predictions, at constant absorbed power, with those demonstrated by LASNEX. Emphasis is placed on successful prediction of the basic quantities of peak ion temperature and compression, rather than neutron yield or $n\tau$.

*Work performed under the auspices of the U.S. Department of Energy by the Lawrence Livermore Laboratory under contract number W-7405-ENG-48.

I. INTRODUCTION

Laser initiated, inertially confined, thermonuclear burn has been described in the literature[1] for lasers that produce on the order of 10 kilojoules in an optimally programmed temporal pulse. The essential characteristics of this process are compression of the thermonuclear fuel to densities on the order of 1000 g/cc, shock heating of the ions at the center of convergence to temperature of 10 keV and thermonuclear bootstrapping of the fuel by redeposition of the burn produced alpha particles to propagate the reaction from the center of convergence. The principal difficulties that are anticipated in achieving these conditions are due to plasma instabilities that may tend to preheat the pellet and make the DT more difficult to compress; and due to hydrodynamic instabilities such as the Rayleigh Taylor instability that tend to destroy the symmetry of the implosion.

In these isentropic implosions, only the exterior of the shell is ablated, causing the interior portion of the shell to be accelerated slowly, resulting in high compression. There are targets, however, that behave in a very different way. These are known as "exploding-pushers,"[2] in which an intense laser pulse rapidly heats a glass microballoon which contains DT gas. The energy deposition, via the electrons, occurs so quickly that the glass shell explodes. Roughly half its mass explodes outward, and the remaining half, inward. The imploding half of the shell acts as a piston, driving a shock through the DT that principally heats the ions. The glass shell then continues to move inward, adiabatically

compressing the post-shock region of DT, thus further heating the ions to thermonuclear temperatures.

Fig. (1) is a typical pressure-density path for a DT fluid element in an exploding pusher target. Note the steep non-adiabatic rise in pressure, as the initial electron-thermal wave sweeps into the DT, raising T_e more rapidly than T_i. The isothermal shock ($\gamma = 1$) followed by adiabatic compression ($\gamma = 5/3$) are clearly seen. The implosion culminates when the impulse generated by the compressed DT stops the inward moving glass. For comparison, the Fermi-degenerate adiabat is shown, which near isentropic compressions should approximate.

Thus, in sharp contrast to high compression, isentropic implosion targets, exploding pushers are much less sensitive to superthermal electron preheat, and, by virtue of their non-ablative implosion dynamics, much less susceptible to hydrodynamic instabilities. In addition, the laser pulse may be a simple gaussian of moderate energy, and the illumination may be relatively asymmetric. A variety of emissions from the imploded target, including x-rays, neutrons, alpha particles, ions, and scattered light, make detailed diagnostics possible. These targets are relatively simple to fabricate, as well. All these factors have made exploding pusher targets the best suited candidates for both early laser-fusion studies, and for the first targets to be shot on the SHIVA laser system.

In the next section we briefly describe the SHIVA laser system and propose a method of achieving high efficiency of laser light absorption

into the target. In section III the relevant model physics of the computer code LASNEX[3] is described. Section IV deals with the results of the design study, in which shell thickness and radius, DT fill, and laser pulse length were varied to find optimal targets in both yield and gain (≡ yield/incident laser energy). Section V briefly lays forth some simple theories on scaling rules for exploding pushers, which are compared with LASNEX results in section VI.

II. ABSORPTION OF THE SHIVA LASER LIGHT

The SHIVA laser system is designed to produce over 20 TW of power from 20 simultaneously fired laser chains. The wavelength of the light is 1.06 μm, originating from a Nd:YAG laser.

Recent experiments at Lawrence Livermore Laboratory[4] have confirmed theoretical predictions[5] of resonant absorption of laser light, whose significant feature is the absorption peak near 20° with nearly 50% absorption for p-polarized light. Because of the spherical geometry of our target, and the fact that we have 20 separate beams, we can polarize each beam so that it will be p-polarized and have nearly a 20° inclination (from normal incidence) towards the local surface of the sphere upon which it is incident. Thus with the SHIVA laser system we hope to approach 50% absorption on these simple exploding pusher targets.

III. DESCRIPTION OF LASNEX PHYSICS

The LASNEX code used to design and interpret the experiments allows the hydrodynamic, transport, atomic and nuclear processes occurring within the target plasma to be calculated as a function of time and two spatial coordinates. We outline here some of its essential features. Geometrical ray tracing is used to calculate the focal, refractive and reflective properties of the laser pulse. Laser light is absorbed by inverse bremsstrahlung, resonance absorption and parametric decay instabilities.

Energy absorbed by resonance and parametric processes is used to promote thermal electrons into a higher energy (assumed Maxwellian) distribution characterized by a temperature α times the thermal temperature. The electrons heated by inverse bremsstrahlung are placed in a softer distribution characteristic of that process. The resulting non-Maxwellian electron distribution is transported by multi-group flux-limited diffusion techniques. These electrons lose energy by Coulomb collisions with cooler thermal electrons and by doing work on the self-consistent electric field set up to enforce charge neutrality. Thermal electron conductivity is flux-limited and adjusted to account for plasma turbulence and magnetic fields generated by circulating electron currents. Bound-bound, bound-free, and free-free radiative processes are calculated assuming that the bound state populations are those of average atoms in LTE with the thermal electrons. Photons so produced are transported by multi-group, flux-limited diffusion and frequency shifted by Doppler and Compton effects. The hydrodynamic calculation involves partial pressures from all plasma components as well

as magnetic, real and artificial viscous stresses. In addition to electron Coulomb collisions, thermal ions are heated by viscous and hydrodynamic work. Diffusion of these ions through the plasma results in ion heat conduction and the mixing of different ionic species. Maxwell averaged cross sections are used to calculate thermonuclear reaction rates. Neutrons and charged particles produced are transported by multi-group flux-limited diffusion.

IV. DESIGN RESULTS

In order to search through large areas of parameter space, we have run these problems using a one-dimensional approximation, assuming spherical symmetry in both laser irradiation and in implosion. We assume 10 TW absorbed (45% absorption of 22 TW). If SHIVA delivers only 15 TW on its first shot (a more realistic estimate), and thus providing 7 TW of absorbed power to the target, LASNEX predicts that the corresponding yield falls by about a factor of two. This supports a scaling law for exploding pushers of yield with the square of power, $Y \sim P^2$, which has been seen experimentally and has been predicted by LASNEX over a much wider spread of powers (1-100 TW).

The laser's temporal behavior is set to a gaussian whose FWHM is varied between 60 and 150 ps. The target size is varied in both radius and glass shell thickness. The DT fill is held fixed at 5 mg/cc. It should be reiterated, at this point, that the simple targets we explore here are by no means the best possible performers for the SHIVA system, but rather the best for the first shot - they are relatively simple to construct and diagnose and do not make stringent demands on the laser system (i.e., they do not require sophisticated pulse shaping).

Figs. (2)-(4) show the results of LASNEX calculations for a pulse width of 60, 100, and 150 ps respectively. Though the 100 ps (2100 j) pulse, 300 μm diameter, 2.5 μm thick target wins the neutron derby, with 2.4 trillion neutrons, its gain is only 0.3%. The shorter pulse, 60 ps

(1280 j), 250 μm diameter, 2.5 μm thick target has a gain of 0.4% despite its lower yield.

Fig. (5) shows a slightly more complex laser pulse - a square top created by stacking 30 ps gaussians. With this pulse the yield rises to 3 trillion neutrons. Fig. (6) relates both the yield and gain of two such targets when the square top is cut off after some finite time.

A full two-dimensional calculation of a SHIVA target is beyond the scope of this present work. Results for a DT fill of 2 mg/cc give similar numbers, with optima slightly lower than the 5 mg/cc case.

V. SCALING THEORIES

A number of different theories for the exploding pusher have appeared recently. In this paper we concentrate on that of Nuckolls[6] while exploring some possible modifications to that theory.

In order to calculate the yield of the target we note that

$$Y \sim Mn\overline{\sigma v}\tau_c \tag{1}$$

where M is the mass of the DT, n its number density, $\overline{\sigma v}$ is the product of velocity and fusion cross sections averaged over a Maxwellian distribution, and τ_c is the confinement time. Now $M \sim \rho_0 R_0^3$ where ρ_0 is the initial DT fill density, and R_0 the initial radius, and $n \sim \rho_0 \eta$ where η is the compression ratio, $(R_0/R_F)^3$. The confinement time is given, in most cases of interest, by $\tau_c \sim R_F/c_s \sim R_0/(\eta^{1/3}\theta_i^{1/2})$ where θ_i is the DT ion temperature at compression. Thus

$$Y \sim \rho_0^2 R_0^4 \eta^{2/3}(\overline{\sigma v}/\theta_i^{1/2}) \ . \tag{2}$$

Since $\overline{\sigma v}$ is a known function of θ_i, we must derive expressions for the compressions η and the peak ion temperature θ_i.

The estimate for η is based on the definition of an exploding pusher, in that we assume that 1/2 the mass of the glass shell explosed inward, eventually filling almost all of the interior volume. Implicit in this assumption is that $\eta^{-1/3} \equiv (R_F/R_0) \ll 1$. Since compressions are typically 100, this condition is fairly well satisfied. In Appendix A we derive, from a dynamic point of view, why compressions are of this order. Conservation

of this glass mass then immediately yields

$$\overline{\rho_g} = 4(\Delta R/R) \tag{3}$$

where ρ_g is the average glass density at the time of peak compression, and ΔR is the initial width of the glass shell. The central glass density, ρ_{gc}, is higher than this average at turn around time. The final DT density, ρ_F, is roughly equal to the central glass density because the pressures are equal at the glass-DT interface, and thermal conduction equalizes the temperatures as well. Empirically then Nuckolls' finds that Eq. (3) leads to

$$\rho_F \approx \rho_{gc} \approx 16\ (\Delta R/R) \tag{4}$$

giving

$$\eta \approx 16\ \frac{\Delta R}{R\rho_0} \tag{5}$$

where the factor of 4 is presumably due to the difference between central and average glass densities.

A closer look at this problem allows the analysis to proceed one step further. The density profile of the glass at turn around time, as calculated by LASNEX is shown in Fig. (7). Roughly it is $\rho \sim (1/r^2)$. This is quite plausible since conservation of mass tells us that

$$\frac{\partial \rho}{\partial t} + \frac{1}{r^2}\ \frac{\partial}{\partial r}\ (r^2 \rho v_r) = 0 \tag{6}$$

At turn around time, $(\partial\rho/\partial t) \approx 0$ since we are at an extremum. The radial velocity v_r is roughly flat at this time, leaving $\rho \sim (1/r^2)$. With this

definite profile, we can explicitly calculate the average $\bar{\rho}_g$ and its relationship to the central density ρ_{gc}. We obtain

$$\rho_g \approx (\eta^{-1/3})\, \rho_{gc} \tag{7}$$

Then

$$\rho_F \approx \rho_{gc} \approx \eta^{1/3}\rho_g \approx 4\, \eta^{1/3}(\underline{\Delta R}/R).$$

But $\rho_F = \eta\rho_o$, therefore

$$\eta \approx 8\, (\Delta R/R\rho_o)^{3/2} \tag{8}$$

giving a different scaling for η than Eq. (5).

As a caveat we mention certain details left out of the above calculation.

1. The DT density does not exactly match the glass density at the interface, despite the equality of pressure and temperatures. This is due to their different Zs.

2. The DT density profile is not flat either at turn around time, it rises as it approaches the interface. This is due to v_r being close to zero at the interface, at turn around time (See Eq. (6)).

3. The glass profile is not strictly $(1/r^2)$, also due to variations in v_r, and small deviations from the $(1/r^2)$ behavior change eq. (7) into

a transcendental equation in η and thus effectively change the coefficient in Eq. (8), and, to a lesser degree, the scaling.

We now proceed to calculate θ_i, the peak ion temperature. As was shown in Fig. (1) the ion heating proceeds in three stages. An electron thermal wave heats the DT electrons, and, because the coupling is weak in the diffuse gas, these slightly heat the ions. In the glass however, the coupling is strong, and the hot glass ions explode inward and shock the DT ions. The glass continues inward, adiabatically compressing the post-shock region of DT. If we denote the post-shock temperature as θ_{ps} then

$$\theta_i = \theta_{ps}\eta^{\gamma-1} \tag{9}$$

Though γ should theoretically be 5/3, because of conduction losses it can vary. This variation can easily frustrate any attempt at proving a scaling law.

Behind a strong shock the internal energy matches the kinetic energy, and $\rho_{p.s.} = 4\rho_o$, so if V_o is the initial explosion velocity of the inwardly moving glass ions we get

$$\theta_{ps} \sim V_o^2 \tag{10}$$

But $V_o^2 \sim (P\tau_L)/(R_o^2\Delta R)$ where P is the laser power, τ_L is the effective absorption time, and $R_o^2\Delta R$ represent the mass of the pusher. Thus

$$\theta_i \sim (P\tau_L)\eta^{\gamma-1}/(R_o^2\Delta R). \tag{11}$$

Since η is given in terms of ρ_0, R_0, ΔR by either Eq. (5) or (8), θ_i can be determined once τ_L is designated. There are a number of possibilities. First, τ_L could be the FWHM of the gaussian. However, this cannot be true for all targets since a small target implodes too quickly, and not all of the laser's energy is effectively absorbed and converted into V_0. (If, on the other hand, the target is too massive, it probably won't be an exploding pusher!) Another possibility, useful in exploring only the optimal targets at each power level, is to claim that $\tau_L \sim R_0/\theta_i^{1/2}$. This is equivalent to saying that the time scale for laser energy input is roughly the same as the hydrodynamic timescale, i.e. a given pulse will have an optimal target associated with it whose size is well tailored to it. However, in this paper we concentrate on a given power level, so that this formulation of τ_L can only apply to the select few of the targets that are optimal (one for each FWHM chosen for study).

Another possibility is to define an explosion time, τ_{EX}, in which the glass moves a distance comparable to its initial thickness, and set $\tau_L = \tau_{EX}$. This is a statement that after such a time, additional energy deposition is useless, as the explosion has already taken place. Thus $\tau_L = \tau_{EX} \sim (\Delta R/c_s) \sim (\Delta R)\cdot(P\tau_{EX}/R^2\Delta R)^{-1/2}$. Then $\tau_L \sim \Delta R\, R^{2/3}P^{-1/3}$.

Yet another possibility is to set τ_L proportional to $R/c_s \sim R\cdot(P\tau_L/R^2\Delta R)^{-1/2}$. This states that after the shell moves inward an appreciable amount of the remaining energy deposited by the laser cannot reach the moving interface, and is therefore useless. We then obtain

$$\tau_L \sim R^{4/3} \Delta R^{1/3} p^{-1/3} .$$

With these different models for τ_L, we can, via Eq. (11), find θ_i in terms of the input parameters ρ(Fixed), R_o, ΔR, and ρ_o. Then with either Eq. (5) or (8) for $\eta = \eta\ (R_o, \Delta R, \rho_o)$ we can predict the scaling of yield, Eq. (2). Table I is a summary of these different possibilities. Once θ_i is known, we represent $\overline{\sigma v}/\theta_i^{1/2}$ as $\theta_i^{x-1/2}$. Fig. (8) shows how $\overline{\sigma v}$ varies with temperature, by plotting T vs. X. Calling y = x-1/2, Table II shows the scaling of yield with input parameters, depending on τ_L models Table IIb, Eq. (5) column seems most esthetically pleasing at this point. When y = 3 the yield becomes independent of ρ_o, R_o, and ΔR simultaneously, implying a true optimum. ($\partial Y/\partial \rho_o = \partial Y/\partial R_o = \partial Y/\partial \Delta R = 0$). In addition, $Y \sim p^{2y/3} \sim p^2$ which, as mentioned earlier, seems to hold over a wide range of powers. From Fig. (8), we see that $y = 3 \Rightarrow x = 3.5 \Rightarrow \theta_i = 5.5$ keV as the optimal temperature for these optimal targets. Since LASNEX calculations show optima at many different temperatures (for different powers) this seems questionable.

In any event it is clear that the yield is a complex conglomeration of R_o, ρ_o, ΔR and it appears difficult to pick a single model that will explain yield behavior for fixed absorbed power. In the next section we will look at LASNEX results for 10 TW absorbed, and try to ascertain which of these models best describes the exploding pusher target by investigating the more basic quantities of η and θ_i.

VI. LASNEX SCALING

Aside from optimization studies we have also done some scaling studies, deliberately going in the off-optima direction to test the models presented in Section V. We first present scaling with fill density, ρ_o, for fixed R_o, ΔR, and, as always in this paper, fixed power P. We then choose other R_o, ΔR targets and vary ρ_o again, and so on. We find a scaling of $\eta \sim \rho_o^{-6/5}$. This is exactly midway between the scaling of Eqs. (5) and (8), so at first glance determines neither as the correct model. However this scaling is qualitatively closer to Eq. (8), in that for fixed $\Delta R/R$, the final DT density ρ_F ($= \eta\rho_o$) decreases as ρ_o increases, an interesting phenomenon which can only come about with η varying more strongly with ρ_o than $1/\rho_o$.

In the same series of runs we check θ_i and find $\theta_i \sim 1/\rho_o$. From Table I, a, c, and d, we see that this result also supports Eq. (8) over Eq. (5).

The next parameter to check is η and θ_i vs. ΔR, for fixed ρ_o, R_o, and P. Typically ΔR is varied from 1 to 3 μ (to ensure that we are still in the exploding pusher regime) so the quantitative scaling should be taken with an appropriate grain of salt. While η again averages midway between Eqs. (5) and (8), $\eta \sim (\Delta R)^{6/5}$, the more interesting and revealing behavior is the θ_i dependence which first rises with ΔR at low ΔRs, reaches an optimum, and then falls with increasing ΔR. Since each of our models predicts only one of these three behaviors, no single one of them

can hold globally. As such we can not really expect to find a simple scaling model at fixed power. However, qualitatively, the θ_i behavior can be understood in terms of our simple models. For small ΔRs, the explosion happens quickly, so τ_L is not the FWHM of the Gaussian (model a of Table I) but rather it is a limited τ_L since all the laser energy is not effectively used. These are represented by models c or d of Table I which show θ_i increasing with ΔR (Except for Eq. (5) and model d, which is, at least, flat in ΔR). For thicker shells, the total energy is effectively deposited and models a and b of Table I should hold. This indeed happens, as Eq. (8) predicts flat behavior in ΔR, while Eq. (5) even predicts the later behavior of θ_i falling with increasing ΔR.

Thus these different regimes frustrate our efforts at a unified simple model for exploding pushers.

When we study η and θ_i vs. R_o a similar phenomenon occurs, and two regimes are clearly seen. Near the optimal ΔRs (for each R_o studied) we find that $\eta \sim R_o^{-3/2}$ and $\theta_i \sim R_o^{-3/2}$. The η behavior firmly confirms Eq. (8) while the θ_i behavior is too ambiguous to pick out any model in particular. Though it possibly follows model (d), and in between the predictions of Eq. (5), $R_o^{-4/3}$, and Eq. (8), $R_o^{-5/3}$. On the thick ΔR targets (for each R_o studied) we find $\eta \sim \theta_i \sim 1/R_o^3$. The compression falls more rapidly in this regime as some ablation occurs in these thick targets, before the explosion. Thus effectively less than half of the glass mass is imploded and subsequently there is less compression than is to be expected by our models (Eqs. (5) or (8)). The temperature behavior $\theta_i \sim R_o^{-3}$ is predicted by model a and Eq. (8). As discussed earlier, model a for τ_L is quite reasonable in this thick ΔR regime.

VII. CONCLUSIONS

Exploding pusher targets are relatively simple to construct, insensitive to electron preheat and hydrodynamic instability problems, and do not require sophisticated laser pulse shaping. As such they are ideal as a first target for the SHIVA laser system. We find optimal targets that yield over 2 trillion neutrons and are within about one-half of one percent of scientific breakeven.

We have checked simple models of the physics of exploding pushers by comparing their scaling predictions, at fixed power, with those demonstrated by LASNEX. The compression is determined not only by the fact that one-half of the shall mass explodes inward, but also by the density profile of the glass at turn around time, leading to Eq. (8). The ion temperature is raised to thermonuclear levels by shock heating followed by adiabatic compression. The shock heating, characterized by the shell's V_0, is sensitive as to whether or not all of the laser energy was utilized in creating the shell's explosion. This leads to the different regimes of thin and thick shelled exploding pushers, in which effective laser energy or full laser energy is taken into account. This prevents us from writing simple scaling laws for the yield, at fixed absorbed power.

It bears repeating that another effect frustrates our efforts at proving a model by its agreement with LASNEX. Conduction effects change the effective γ, and it can vary from 1.5 to 2. This is enough to radically change most of the scaling predictions of most of the simple models.

Despite this difficulty we have shown here that our simple ideas on exploding pushers stand up relatively well to the results of the complex LASNEX code.

APPENDIX A

Compression Calculation from the Point of View of Shell and Shock Dynamics

In an exploding pusher the shell moves inward rapidly, almost acting like a shock itself, while pushing a shock ahead of itself. The shock reflects off of center and meets the incoming shell causing turnaround. The key ansatz we make in this appendix is that both shock and pusher behave as Guderley[7] solutions, $r = \xi t^n$ where $n \approx 0.7$ for $\gamma = 5/3$. They are shown in Fig. (9).

We thus set

$$r_{s_\pm} = r_o\left(\frac{t - T_s}{\mp T_s}\right)^{.7}$$

$$r_{p_\pm} = r_o\left(\frac{t - T_p}{\mp T_p}\right)^{.7}$$

where $r_{s_\pm}$ stands for shock position before and after reflection and $r_{p_\pm}$ for pusher position. They differ due to initial conditions. At $t = 0$, $r_p = r_s = r_o$, but $r_s = u_s = \left((\gamma+1)/2\right)u_p$ and $r_p = u_p$. This is a standard relation in strong shocks.

These initial conditions then imply that $T_s = (0.7)r_o/\left([(\gamma+1)/2]u_p\right)$, and that $T_p = [(\gamma+1)/2]T_s$. At turnaround we have

$$r_{s_-}(t^*) = r_{p_+}(t^*)$$

which yields

$$t^* = \frac{2T_s T_p}{T_s+T_p} = \frac{2(\gamma+1)}{(\gamma+3)} T_s$$

Substituting t* into r we obtain

$$r_{final} = \left(r_o \frac{\gamma-1}{\gamma+3} \right)^{.7}$$

which yields $\eta = (r_o/r_f)^3 = 60$ for $\gamma = 5/3$, a very typical number for exploding pushers. Since γ can effectively vary from 1.5 to 1.8 we get η varying from 102 to 43, well representing the spread in η we obtain during LASNEX optimization runs as we range through parameter space.

TABLE I

	Eq. (5)	Eq. (8)
(a) τ_L = fixed	$\theta_i \sim P(\Delta R)^{-1/3} R_o^{-8/3} \rho_o^{-2/3}$	$\theta_i \sim P\rho_o^{-1} R_o^{-3}$
(b) $\tau_L \sim R/\theta_i^{1/2}$ (optimal targets)	$\theta_i \sim P^{2/3}\Delta R^{-2/9}\rho_o^{-4/9} R_o^{-10/9}$	$\theta_i \sim P^{2/3}\rho_o^{-2/3} R_o^{-4/3}$
(c) $\tau_L \sim \Delta R R^{2/3} P^{-1/3}$ (explosion time, ΔR scale length)	$\theta_i \sim P^{2/3}(\Delta R)^{2/3} R_o^{-2}\rho_o^{-2/3}$	$\theta_i \sim P^{2/3}\Delta R\rho_o^{-1} R^{-7/3}$
(d) $\tau_L \sim R^{4/3}(\Delta R)^{1/3} P^{-1/3}$ (explosion time, R_o scale length)	$\theta_i \sim P^{2/3} R^{-4/3}\rho_o^{-2/3}$	$\theta_i \sim P^{2/3}(\Delta R)^{1/3}\rho_o^{-1} R^{-5/3}$

TABLE II

	Eq. (5)	Eq. (8)
(a) τ_L = fixed	$Y \sim \rho_o^{4/3-2y/3} R_o^{10/3-8y/3} \Delta R^{2/3-y/3}$	$Y \sim \rho_o^{1-y} R_o^{3(1-y)} p^y \Delta R$
(b) $\tau_L \sim R/\theta_i^{1/2}$ (optimal targets)	$Y \sim \rho_o^{4/3-4y/9} R_o^{10/3-10y/9} (\Delta R)^{2/3-2y/9} p^{2y/3}$	$Y \sim \rho_o^{1-2y/3} R^{3-4y/3} \Delta R p^y$
(c) $\tau_L \sim \Delta R\, R^{2/3} p^{-1/3}$ (explosion time, ΔR scale length)	$Y \sim \rho_o^{4/3-2y/3} R_o^{10/3-2y} (\Delta R)^{2/3+2y/3}$	$Y \sim \rho_o^{1-y} R_o^{3-7y/3} (\Delta R)^{1+y} p^{2y/3}$
(d) $\tau_L \sim R^{4/3} (\Delta R)^{1/3} p^{-1/3}$ (explosion time, R_o scale length)	$Y \sim \rho_o^{4/3-2y/3} R_o^{10/3-4y/3} (\Delta R)^{2/3} p^{2y/3}$	$Y \sim \rho_o^{1-y} R_o^{3-5y/3} \Delta R^{1+y/3} p^{2y/3}$

REFERENCES

1. J. Nuckolls, L. Wood, A. Thiessen and G. Zimmerman, Nature (London) 239, 139 (1972).

2. J. H. Nuckolls, UCRL-50000 71-5, 1971 SRD.

3. G. B. Zimmerman, University of California Report No. UCRL-74811, 1973 (unpublished).

4. K. R. Manes, V. C. Rupert, J. M. Auerbach, P. H. Y. Lee, and J. E. Swain, Phys. Rev. Lett. 39, 281 (1977).

5. K. G. Estabrook. E. J. Valeo, and W. L. Kruer, Phys. Fluids 18, 1151 (1975); J. J. Thomson, W. L. Kruer, A. B. Langdon, C. E. Max, and W. C. Mead, UCRL-79628, to be published in Applied Physics Letters.

6. J. Nuckolls, UCRL-79834.

7. G. Guderley, Luftfahrtforschung 19, 302 (1942).

FIGURE CAPTIONS

1. Time evolution of an exploding pusher described by a P-ρ diagram of a DT fluid element. Three phases are thermal wave, shock, and compression. Fermi degenerate adiabat is shown for comparison.

2.-4. Yield vs. ΔR for various R_0s. The FWHMs of the 20 TW gaussian are 60, 100, and 150 ps respectively.

5. Same as Figures 3-5 but with a "square top" 20 TW pulse composed of 30 ps gaussians.

6. Yield and Gain vs. cut-off time of the square top pulse for two targets.

7. Density profile of DT and glass at turnaround time, as determined by LASNEX (solid line) and as idealized (dotted line) to calculate $\overline{\rho_g}$ *in terms of* ρ_{gc}.

8. Ion temperature vs. x where x is defined by $\overline{\sigma v}(T) \sim T^x$.

9. The r-t plots of both the pusher and shock, assuming they both obey Guderley solutions globally.

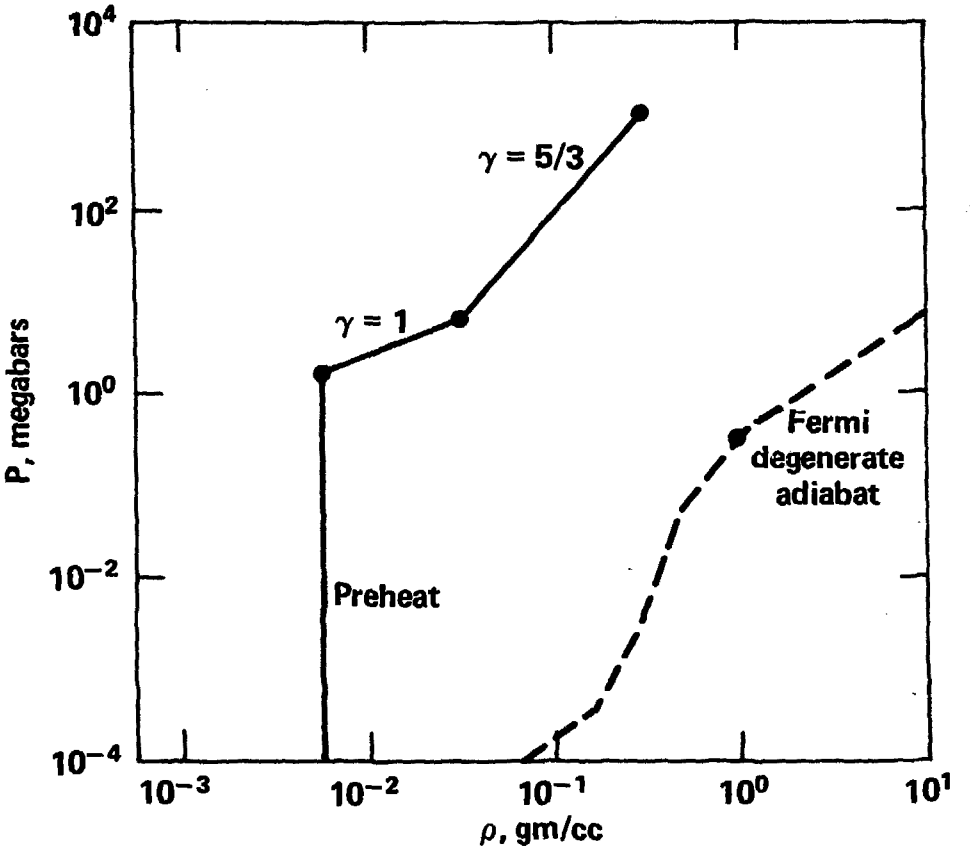
10^4
10^2
10^0
10^{-2}
10^{-4}
P, megabars
$\gamma = 5/3$
$\gamma = 1$
Preheat
Fermi
degenerate
adiabat
10^{-3}
10^{-2}
10^{-1}
10^0
10^1
ρ, gm/cc

9/77

Fig. 1

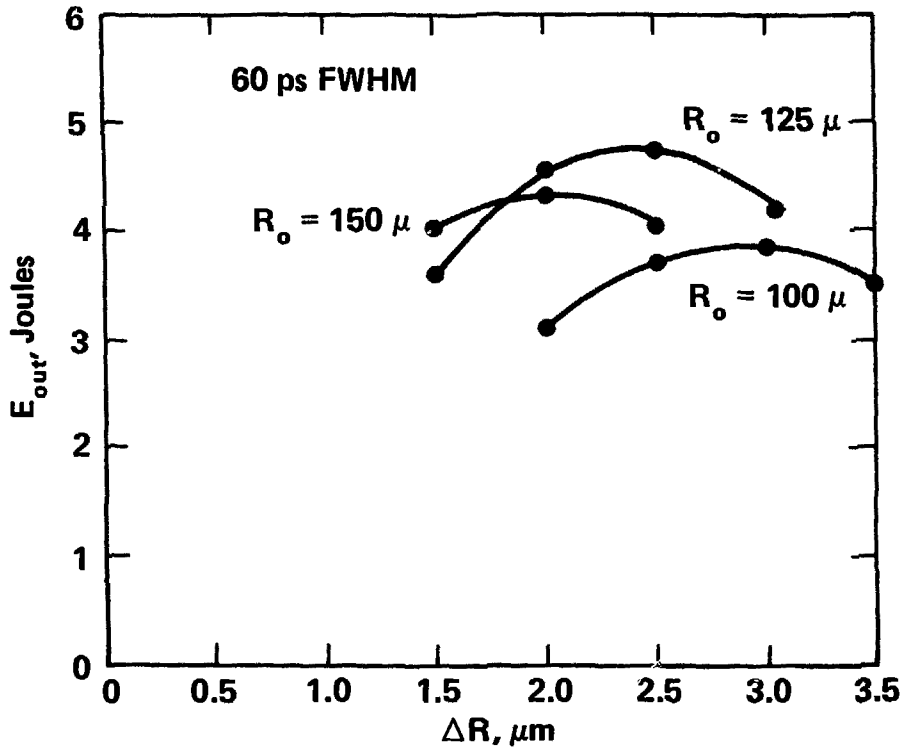
60 ps FWHM
R_o = 125 μ
R_o = 150 μ
R_o = 100 μ
E_{out}, Joules
ΔR, μm
0
1
2
3
4
5
6
0
0.5
1.0
1.5
2.0
2.5
3.0
3.5

9/77

Fig. 2

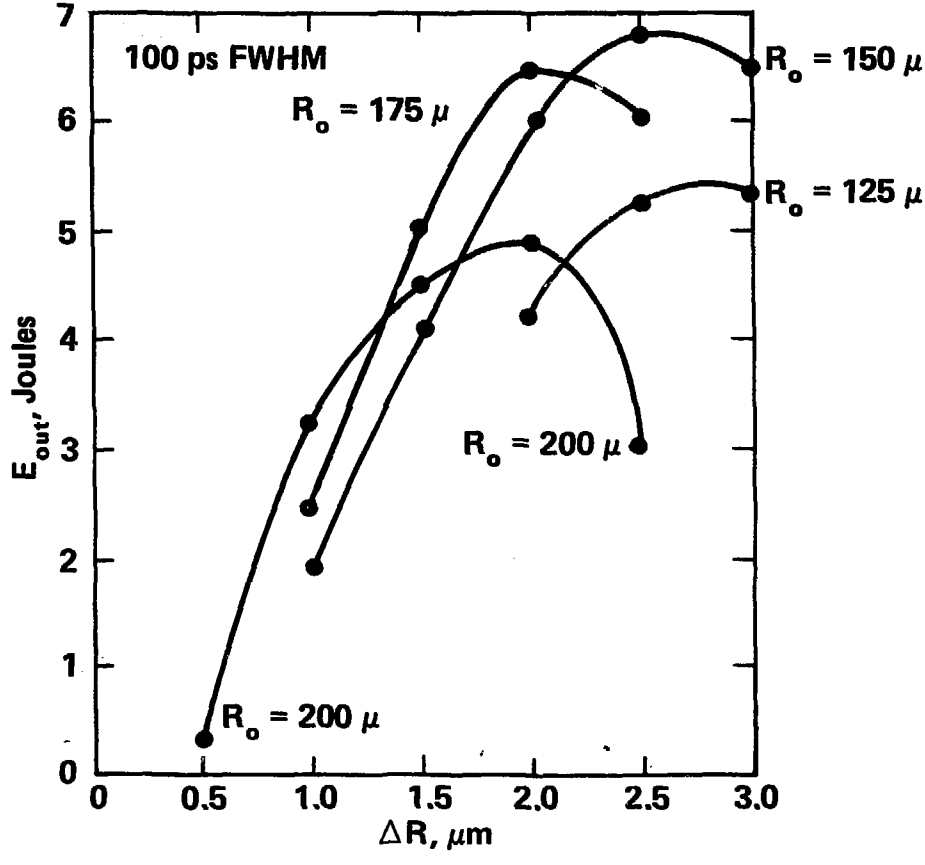
100 ps FWHM
R_o = 175 μ
R_o = 150 μ
R_o = 125 μ
R_o = 200 μ
R_o = 200 μ
E_{out}, Joules
ΔR, μm
0
1
2
3
4
5
6
7
0
0.5
1.0
1.5
2.0
2.5
3.0

9/77

Fig. 3

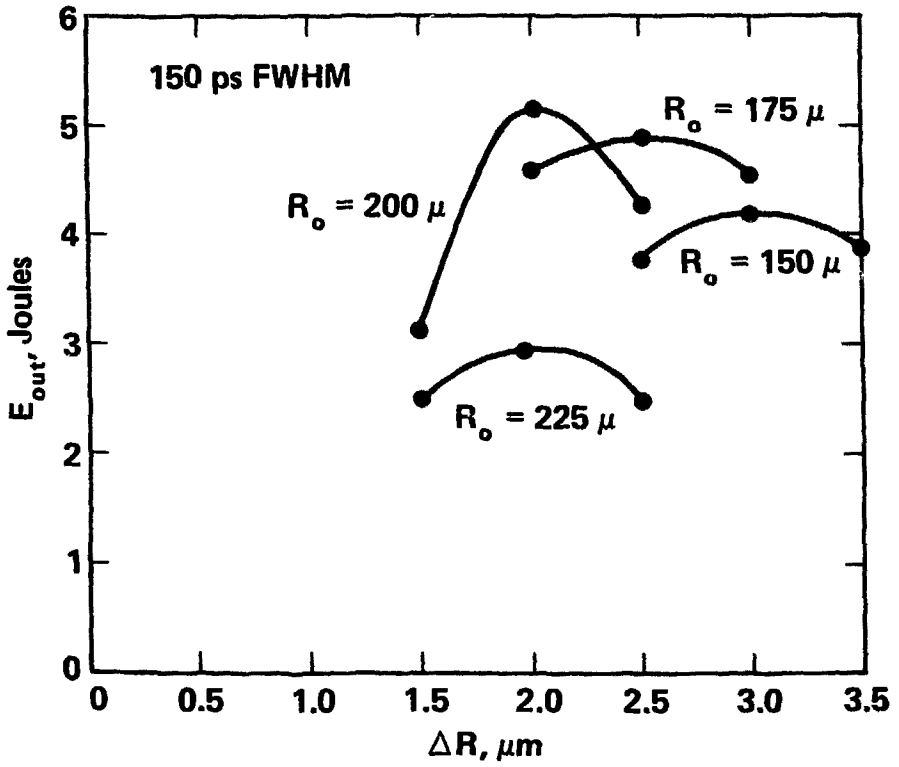
150 ps FWHM
R_o = 175 μ
R_o = 200 μ
R_o = 150 μ
R_o = 225 μ
E_{out}, Joules
ΔR, μm
0
1
2
3
4
5
6
0
0.5
1.0
1.5
2.0
2.5
3.0
3.5

9/77

Fig. 4

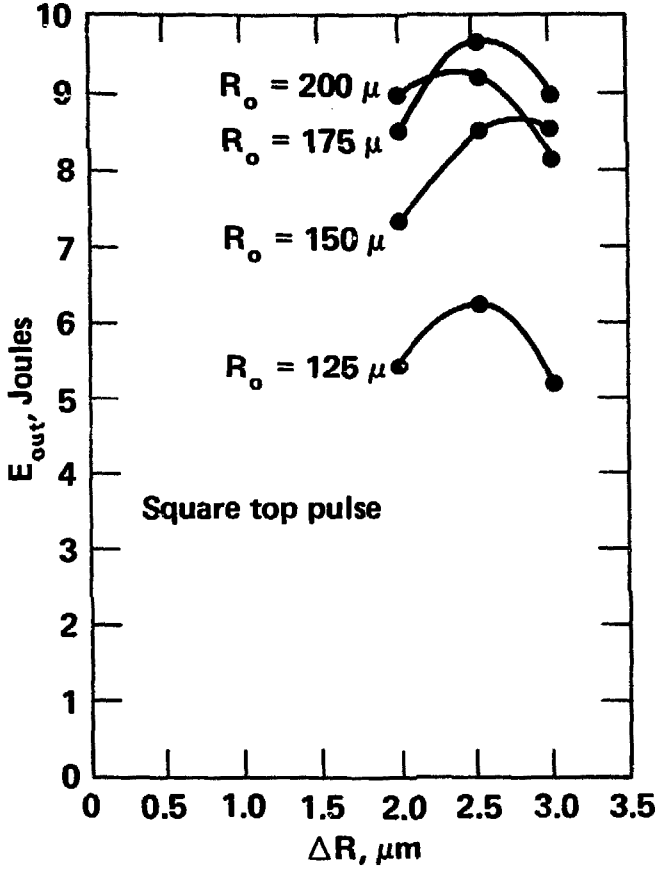
10
9
8
7
6
5
4
3
2
1
0
E_{out}, Joules
R_o = 200 μ
R_o = 175 μ
R_o = 150 μ
R_o = 125 μ
Square top pulse
0
0.5
1.0
1.5
2.0
2.5
3.0
3.5
ΔR, μm

9/77

Fig. 5

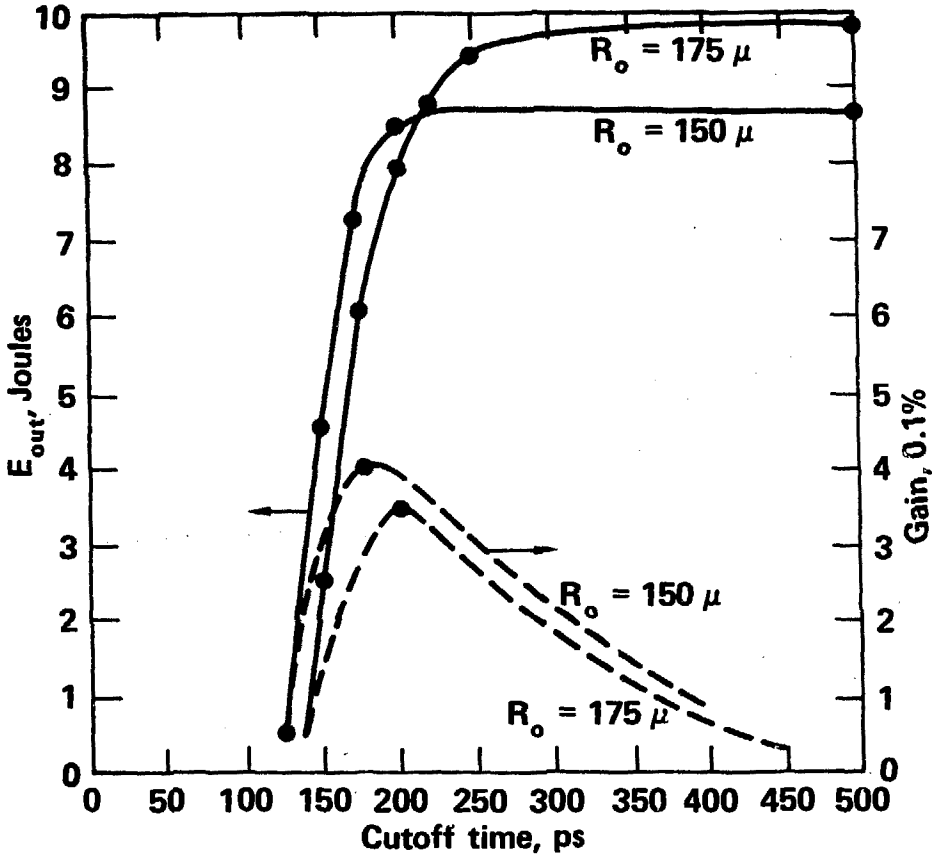
R_o = 175 μ
R_o = 150 μ
R_o = 150 μ
R_o = 175 μ
E_{out}, Joules
Gain, 0.1%
Cutoff time, ps
0
50
100
150
200
250
300
350
400
450
500
1
2
3
4
5
6
7
8
9
10

9/77

Fig. 6

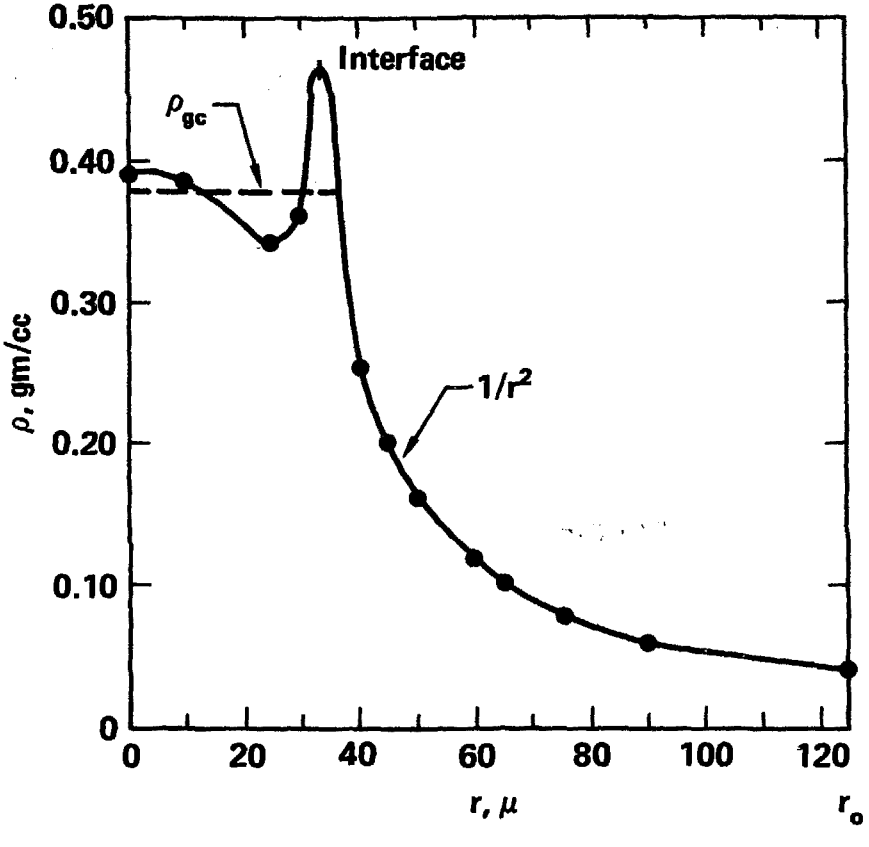
0.50
0.40
0.30
0.20
0.10
0
Interface
ρ_{gc}
$1/r^2$
ρ, gm/cc
0
20
40
60
80
100
120
r, μ
r_o

9/77

Fig. 7

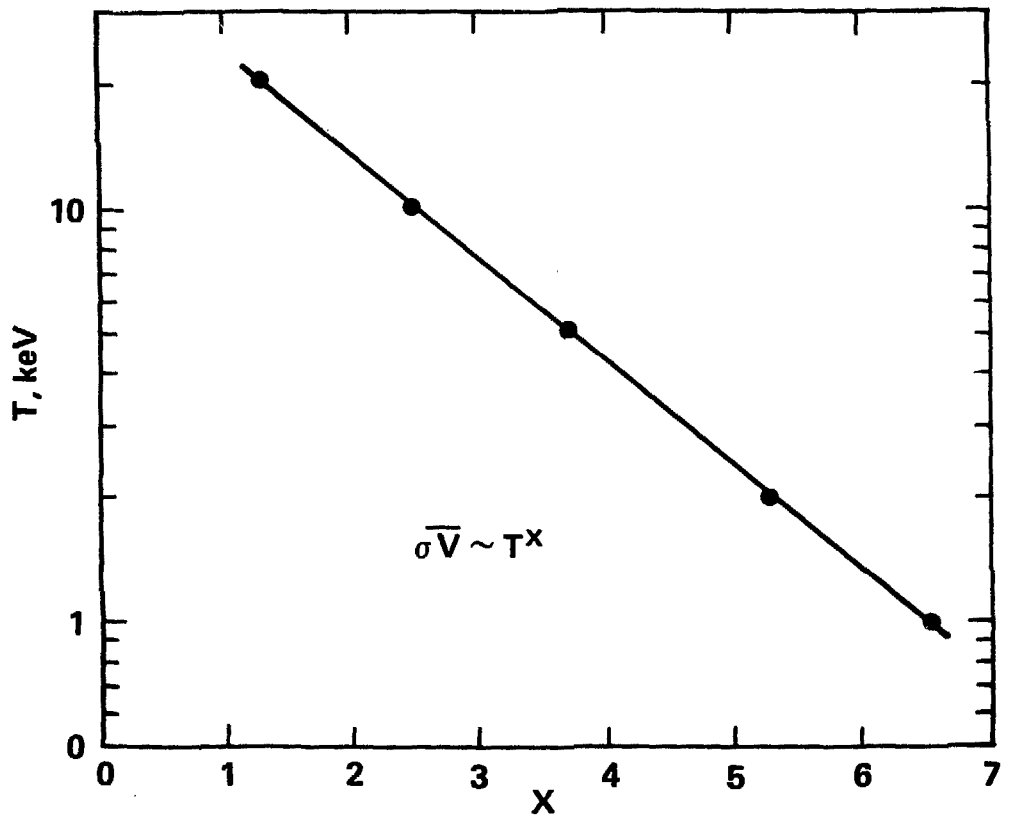

9/77

Fig. 8

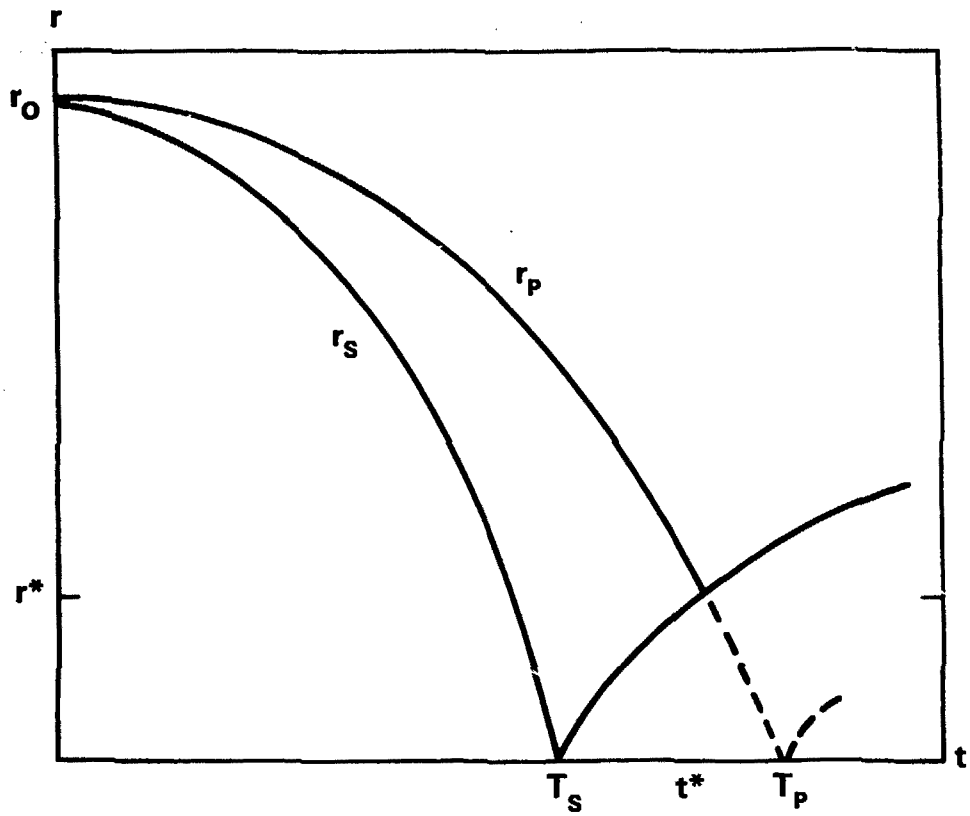

9/77

Fig. 9

Distribution

M. D. Rosen (50 copies) L-477

T.I.D. (15 copies)

T.I.C., Oak Ridge (2 copies)

DOE/DLF (21 copies)